Frontiers of Information Technology & Electronic Engineering
www.jzus.zju.edu.cn; engineering.cae.cn; www.springerlink.com
ISSN 2095-9184 (print); ISSN 2095-9230 (online)
E-mail: jzus@zju.edu.cn

Numerical study of a bi-directional in-band pumped dysprosium-doped fluoride fiber laser at 3.2 μm*

Lingjing LI§1, Chunyang MA§2, Nian ZHAO1, Jie PENG1, Bin LIU1,
Haining JI1, Yuchen WANG‡3, Pinghua TANG‡1

[1]School of Physics and Optoelectronics, Xiangtan University, Xiangtan 411105, China
[2]Research Center of Circuits and Systems, Peng Cheng Laboratory, Shenzhen 518055, China
[3]Shanghai Institute of Optics and Fine Mechanics, Chinese Academy of Sciences, Shanghai 201899, China
E-mail: 201705710111@smail.xtu.edu.cn; macy15@foxmail.com; nzhao@xtu.edu.cn; jpeng@xtu.edu.cn; liubin@xtu.edu.cn; sdytjhn@xtu.edu.cn; wangyuchen@siom.ac.cn; pinghuatang@xtu.edu.cn

Received Oct. 16, 2023; Revision accepted Nov. 26, 2023; Crosschecked June 3, 2024

Abstract: Dy^{3+}-doped fluoride fiber lasers have important applications in environment monitoring, real-time sensing, and polymer processing. At present, achieving a high-efficiency and high-power Dy^{3+}-doped fluoride fiber laser in the mid-infrared (mid-IR) region over 3 μm is a scientific and technological frontier. Typically, Dy^{3+}-doped fluoride fiber lasers use a unidirectional pumping method, which suffers from the drawback of high thermal loading density on the fiber tips, thus limiting power scalability. In this study, a bi-directional in-band pumping scheme, to address the limitations of output power scaling and to enhance the efficiency of the Dy^{3+}-doped fluoride fiber laser at 3.2 μm, is investigated numerically based on rate equations and propagation equations. Detailed simulation results reveal that the optical–optical efficiency of the bi-directional in-band pumped Dy^{3+}-doped fluoride fiber laser can reach 75.1%, approaching the Stokes limit of 87.3%. The potential for further improvement of the efficiency of the Dy^{3+}-doped fluoride fiber laser is also discussed. The bi-directional pumping scheme offers the intrinsic advantage of mitigating the thermal load on the fiber tips, unlike unidirectional pumping, in addition to its high efficiency. As a result, it is expected to significantly scale the power output of Dy^{3+}-doped fluoride fiber lasers in the mid-IR regime.

Key words: Mid-infrared laser; Fiber laser; Bi-directional pumping
https://doi.org/10.1631/FITEE.2300701 **CLC number:** TN248

1 Introduction

Lasers operating in the mid-infrared (mid-IR) wavelength regime at around 3 μm have gained significant interest due to their important applications in environment monitoring, biomedicine, molecular spectroscopy, and infrared countermeasures (Ilev and Waynant, 2006; Sijan, 2009; Jackson, 2012; Ycas et al., 2018). Among them, fiber lasers stand out due to their excellent beam quality, long-term stability, and scalability for high power output (Shen et al., 2017).

Typically, ~3 μm mid-IR fiber lasers can be generated using Er^{3+}-, Ho^{3+}-, and Dy^{3+}-doped fluoride fibers (Jackson, 2012; Li et al., 2012; Aydin et al., 2018; Majewski et al., 2020; Wang ZH et al., 2020; Jobin et al., 2022; Luo et al., 2022, 2023; Pajewsk et al., 2023). The Ho^{3+}-doped fluoride fiber laser, pumped by a 1150-nm laser diode, has achieved continuous-wave

§ These authors contributed equally to this work
‡ Corresponding authors
* Project supported by the Hunan Provincial Natural Science Foundation of China (Nos. 2023JJ30596 and 2022JJ30556), the Scientific Research Fund of Hunan Provincial Education Department, China (No. 21B0136), the National Natural Science Foundation of China (No. 62105209), the Shanghai Pujiang Program, China (No. 22PJ1414900), and the Shenzhen Government's Plan of Science and Technology, China (No. RCYX20210609103157071)
ORCID: Yuchen WANG, https://orcid.org/0000-0002-5815-1755; Pinghua TANG, https://orcid.org/0000-0003-2285-9812

(CW) lasing of >7 W with an optical–optical efficiency of ~30% (Crawford et al., 2015). Similarly, the heavily Er^{3+}-doped fluoride fiber laser has demonstrated an output power of 20.6 W with an optical–optical efficiency of ~36% (Faucher et al., 2011), while recent advancements have pushed its output power beyond 40 W (Aydin et al., 2018). On the other hand, the Dy^{3+}-doped fluoride fiber laser offers a broader emission spectrum (Sójka et al., 2018), demonstrating wide wavelength tunability from 2.8 to 3.4 μm in CW operation (Majewski et al., 2018). This wide emission range bridges the spectra gap between Er^{3+} and Ho^{3+} laser systems of around 2.9 μm and Er^{3+} laser system of around 3.5 μm, which opens up new applications such as real-time sensing and polymer processing (Majewski et al., 2020, 2021). Furthermore, the Dy^{3+}-doped fluoride fiber laser offers flexibility in terms of pump source selection (Amin et al., 2020), enabling the use of 1.1-, 1.3-, 1.7-, and 2.8-μm wavelengths as pump sources (Jackson, 2003; Tsang et al., 2006; Tsang and El-Taher, 2011; Majewski and Jackson, 2016; Majewski et al., 2018, 2021; Woodward et al., 2018; Fortin et al., 2019; Wang YZ et al., 2022; Xiao et al., 2024). These characteristics make Dy^{3+}-doped fluoride fiber a compelling choice as a gain fiber for generating mid-IR fiber lasers, especially in the >3 μm region.

Among the available pump sources, the 2.8-μm laser stands out as a particularly attractive option for achieving high-efficiency and high-power Dy^{3+}-doped fluoride fiber lasers due to the low quantum losses, simple conversion, and high conversion efficiency of the in-band pumping (Majewski et al., 2019, 2021; Jobin et al., 2020; Tang et al., 2022; Zhang et al., 2022). Researchers have achieved notable results using this pumping scheme, such as an optical–optical efficiency of ~27% with an output power of ~100 mW (Majewski and Jackson, 2016) and ~190 mW (Majewski et al., 2019), an optical–optical efficiency of ~66% with a maximum output power of 1.06 W (Woodward et al., 2018), and an optical–optical efficiency of ~53% with a maximum output power of 10.1 W (the highest reported output power from a Dy^{3+}-doped fluoride fiber laser to date) (Fortin et al., 2019). However, it is worth noting that all the previously reported 2.8-μm in-band pumped Dy^{3+}-doped fluoride fiber lasers employ a unidirectional pumping scheme, which still faces significant challenges in terms of thermal loading density on the fluoride gain fiber tips in the high launched pumped power regime. This thermal effect has the potential to cause damage and places limitations on the scalability of output power, unlike its silica counterparts, which boast much higher damage thresholds.

To address the limitations of output power scaling and improve the efficiency of the Dy^{3+}-doped fluoride fiber lasers, a bi-directional in-band pumping scheme is proposed and numerically investigated in this work. In this pumping scheme, equal pump power is injected from both ends of the gain fiber, effectively mitigating the thermal effect on the fiber tips more than unidirectional pumping does with the same total pump power, thus offering significant potential for the high-power operation of fluoride fiber lasers. Detailed simulation results reveal that the optical–optical efficiency of the bi-directional in-band pumped Dy^{3+}-doped fluoride fiber laser can reach 75.1%, which approaches the Stokes limit of 87.3%. The potential for further improvement of efficiency of the Dy^{3+}-doped fluoride fiber laser is also discussed.

2 Numerical model for the simulations

Fig. 1a displays the schematic of the energy-level structure and energy transfer processes relevant to the in-band pumped Dy^{3+}-doped fluoride fiber laser at 3.2 μm. By considering the ground state absorption, stimulated emission, and radiative and nonradiative decays, the rate equations of the in-band pumped Dy^{3+}-doped fluoride fiber laser can be written as follows:

$$\frac{\partial N_1}{\partial t} = -R_{\mathrm{GSA}} N_1 + (R_{\mathrm{SE}} + A_{21} + R_{21}) N_2, \quad (1)$$

$$\frac{\partial N_2}{\partial t} = R_{\mathrm{GSA}} N_1 - (R_{\mathrm{SE}} + A_{21} + R_{21}) N_2, \quad (2)$$

$$N_{\mathrm{Dy}} = N_1 + N_2, \quad (3)$$

where N_1 and N_2 represent the population densities of $^6H_{15/2}$ and $^6H_{13/2}$ levels respectively, N_{Dy} denotes the Dy^{3+} dopant concentration, $A_{21} = \tau_2^{-1}$ and R_{21} are the radiative and nonradiative decay rates from the $^6H_{13/2}$ to $^6H_{15/2}$ level respectively, $R_{\mathrm{GSA}} = R_{\mathrm{GSA}}^{\mathrm{P}} + R_{\mathrm{GSA}}^{\mathrm{S}}$ is the total transition rate associated with the ground state absorption

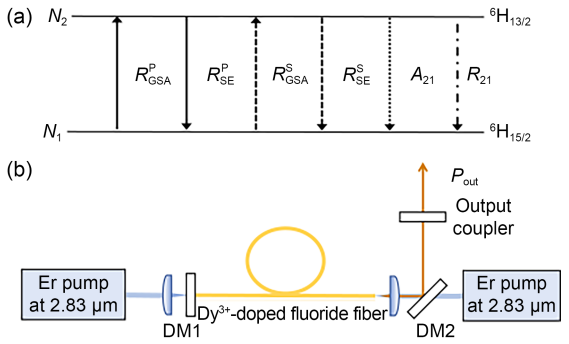

Fig. 1 Energy-level structure and energy transfer processes relevant to the in-band pumped Dy^{3+}-doped fluoride fiber laser at 3.2 μm (a) and the schematic of the fiber laser (b)

(GSA), and $R_{SE}=R^P_{SE}+R^S_{SE}$ represents the total transition rate linked to the stimulated emission (SE). These parameters can be given by

$$R^P_{GSA}=\frac{\sigma_{ap}N_1\Gamma_p}{h\nu_p A_c}\left[P^+_p(z)+P^-_p(z)\right], \quad (4)$$

$$R^P_{SE}=\frac{\sigma_{ep}N_2\Gamma_p}{h\nu_p A_c}\left[P^+_p(z)+P^-_p(z)\right], \quad (5)$$

$$R^S_{GSA}=\frac{\sigma_{as}N_1\Gamma_s}{h\nu_s A_c}\left[P^+_s(z)+P^-_s(z)\right], \quad (6)$$

$$R^S_{SE}=\frac{\sigma_{es}N_2\Gamma_s}{h\nu_s A_c}\left[P^+_s(z)+P^-_s(z)\right]. \quad (7)$$

Here, σ_{ap} and σ_{ep} refer to the absorption and emission cross-sectional area of the atomic transition at the pump wavelength respectively, σ_{as} and σ_{es} represent the absorption and emission cross-sectional area of the atomic transition at the signal wavelength respectively, and Γ_p and Γ_s are the power filling factors for the pump laser and signal laser respectively. For mid-IR Dy^{3+}-doped fluoride fiber lasers, core pumping is commonly employed; thus, Γ_p and Γ_s are set as 0.7511 (Li and Jackson, 2012). h is Planck constant, ν_p is the frequency of the pump laser ($\nu_p=c/\lambda_p$, λ_p is the pump wavelength and c is the speed of light), and ν_s is the frequency of the signal laser ($\nu_s=c/\lambda_s$, λ_s is the signal wavelength). A_c is the effective cross-sectional area of the fiber core, P_p represents the longitudinally varying power of the pump light, and P_s corresponds to the longitudinally varying power of the signal light. The positive and negative signs indicate the forward and backward propagations along the z direction, respectively. The power evolution of the pump and laser light along the propagation direction can be obtained as follows:

$$\frac{dP^+_p(z)}{dz}=-\Gamma_p(\sigma_{ap}N_1-\sigma_{ep}N_2)P^+_p(z)-\alpha P^+_p(z), \quad (8)$$

$$\frac{dP^-_p(z)}{dz}=\Gamma_p(\sigma_{ap}N_1-\sigma_{ep}N_2)P^+_p(z)+\alpha P^+_p(z), \quad (9)$$

$$\frac{dP^+_s(z)}{dz}=\Gamma_s(\sigma_{es}N_2-\sigma_{as}N_1)P^+_s(z)-\alpha P^+_s(z), \quad (10)$$

$$\frac{dP^-_s(z)}{dz}=-\Gamma_s(\sigma_{es}N_2-\sigma_{as}N_1)P^-_s(z)-\alpha P^-_s(z). \quad (11)$$

In these propagation equations, α represents the propagation loss coefficient of the fiber at the pump and signal wavelengths. The pump power and laser power at both fiber ends are subjected to the following boundary conditions (related to Fig. 1b):

$$P^+_p(0)=P^f_0, \quad (12)$$

$$P^-_p(L)=P^b_0, \quad (13)$$

$$P^+_s(0)=R_1P^-_s(0), \quad (14)$$

$$P^-_s(L)=R_2P^+_s(L). \quad (15)$$

Here, P^f_0 and P^b_0 denote the forward and backward pump power launched into the Dy^{3+}-doped fluoride fiber respectively, R_1 and R_2 indicate the reflectivity of the dichroic mirrors DM1 and output coupler (OC) respectively, and L is the fiber length. For the laser systems involved, the output power of the fiber laser is given by

$$P_{out}=(1-R_2)P^+_s(L). \quad (16)$$

Based on the boundary conditions, the rate equations and propagation equations can be solved numerically. The parameters listed in Table 1 are used in the numerical simulations, unless otherwise stated.

In the case of our study, we did not consider Fresnel reflections at the fiber end facets since this concern can be addressed by cleaving the fiber ends with an angle of ~8°. The rate equations (1) and (2) are a typical system of ordinary differential equations, accompanied by four boundary conditions (12)–(15), constituting a two-point boundary value problem (BVP). The commonly used numerical solution methods for BVPs include the shooting method and its improved version (Sujecki, 2014), the relaxation method (Quimby et al., 2008), and the bvp4c function (Woodward and Gorjan, 2022). Here, we employed the MATLAB BVP solver bvp4c directly in the simulations.

3 Numerical results and discussion

To validate the simulation model, we first compare the simulation results with these from the study of Fortin et al. (2019). The simulation parameters, including the fiber and cavity parameters, were set according to the work of Fortin et al. (2019). Fig. 2a presents the simulation results alongside the experimental data of Fortin et al. (2019). The good agreement between them confirms the validity of the numerical model. We then compared the output performances of forward pumping, backward pumping, and bi-directional pumping, with the reflectivity of the OC (R_2) configured at 20% and the fiber length set to 5.5 m. Figs. 2b–2d depict the output power of the Dy^{3+}-doped fluoride fiber laser as a function of incident pump power for each pumping method, revealing that the optical–optical efficiency for bi-directional pumping closely matches that of backward pumping, but surpasses that of forward pumping. Given the intrinsic advantage of bi-directional pumping in mitigating thermal load on the fiber tips, unlike unidirectional pumping, it is believed to hold significant potential for enhancing the output power scaling of Dy^{3+}-doped fluoride fiber lasers with high efficiency in the

Table 1 Parameters used in the simulations

Parameter	Value	Reference
A_c (m^2)	1.2265×10^{-10}	Fortin et al. (2019)
α (dBm^{-1})	0.3	Woodward et al. (2018)
R_1	99%	Woodward et al. (2018)
N_{Dy} (m^{-3})	3.63×10^{25}	Fortin et al. (2019)
λ_p (μm)	2.83	Fortin et al. (2019)
λ_s (μm)	3.2	Fortin et al. (2019)
σ_{ap} (10^{-25} m^2)	3.88	Majewski and Jackson (2016)
σ_{ep} (10^{-25} m^2)	2.05	Majewski and Jackson (2016)
σ_{as} (10^{-25} m^2)	0.26	Majewski and Jackson (2016)
σ_{es} (10^{-25} m^2)	0.68	Majewski and Jackson (2016)
Γ_p	0.7511	Li and Jackson (2012)
Γ_s	0.7511	Li and Jackson (2012)
τ_2 (ms)	13.7	Falconi et al. (2018)
R_{21} (s^{-1})	1539	Falconi et al. (2018)

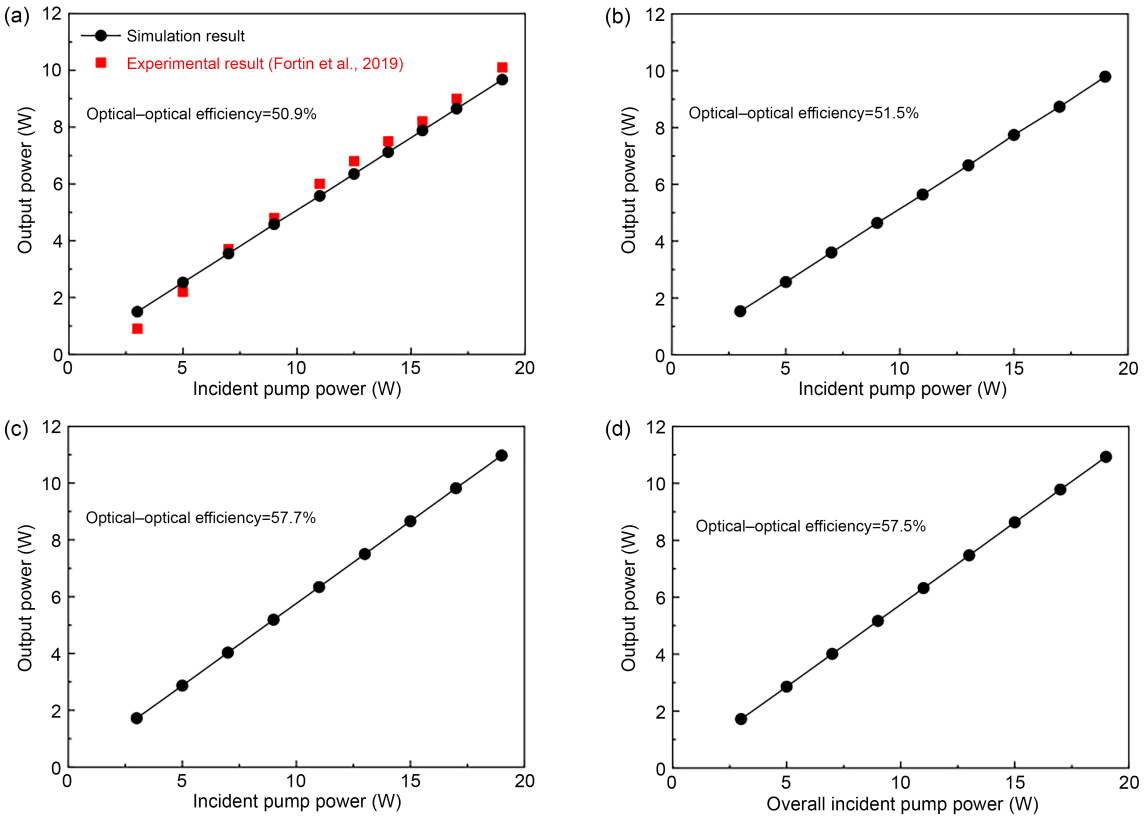

Fig. 2 Comparsion of the simulation results and experimental results from Fortin et al. (2019) (a) and simulated output power of the Dy^{3+}-doped fluoride fiber laser as a function of the incident pump power with different pumping methods: forward pumping (b), backward pumping (c), and bi-directional pumping (d)

high-power regime. Therefore, our study focused on optimizing the output performance of the bi-directional pumped Dy^{3+}-doped fluoride fiber laser.

Next, to optimize the gain fiber length, the dependence of output power and threshold power on the Dy^{3+}-doped fluoride fiber length was investigated. The overall incident pump power was set to 19 W and R_2 was configured at 20%. As depicted in Fig. 3a, a maximum output power of 14.1 W was achieved with a 1.5-m Dy^{3+}-doped fluoride fiber. Beyond this length, the output power starts to decrease, and the laser threshold monotonically increases. Subsequently, the output power and threshold power of the fiber laser with a fixed Dy^{3+}-doped fluoride fiber length of 1.5 m and varying R_2 were studied. The corresponding results as presented in Fig. 3b demonstrate that a relatively high output power can be obtained with the reflectivity within the range of 12%–30%. Additionally, the threshold power decreases as R_2 increases, which is attributed to higher reflectivity, enabling the laser to operate in a lower loss regime. Fig. 3c illustrates the output power versus the Dy^{3+}-doped fluoride fiber length for different R_2 values (12%, 18%, 24%, and 30%). It can be seen that as R_2 decreases, the optimal fiber length increases. By appropriately selecting the fiber length and R_2, a maximum output power of ~14 W can be achieved, which is significantly higher than that presented in the work of Fortin et al. (2019) at the same pump power.

The output power of the bi-directional pumped Dy^{3+}-doped fluoride fiber with respect to the overall incident pump power is shown in Fig. 4. A fiber length of 1.8 m was selected, and R_2 was configured at 12%. The results indicate that the optical–optical efficiency of the fiber laser can reach up to 75.1%, which is close to the Stokes limit of 87.3%.

Additionally, the effect of different dopant concentrations of Dy^{3+}-doped fluoride fiber on the output

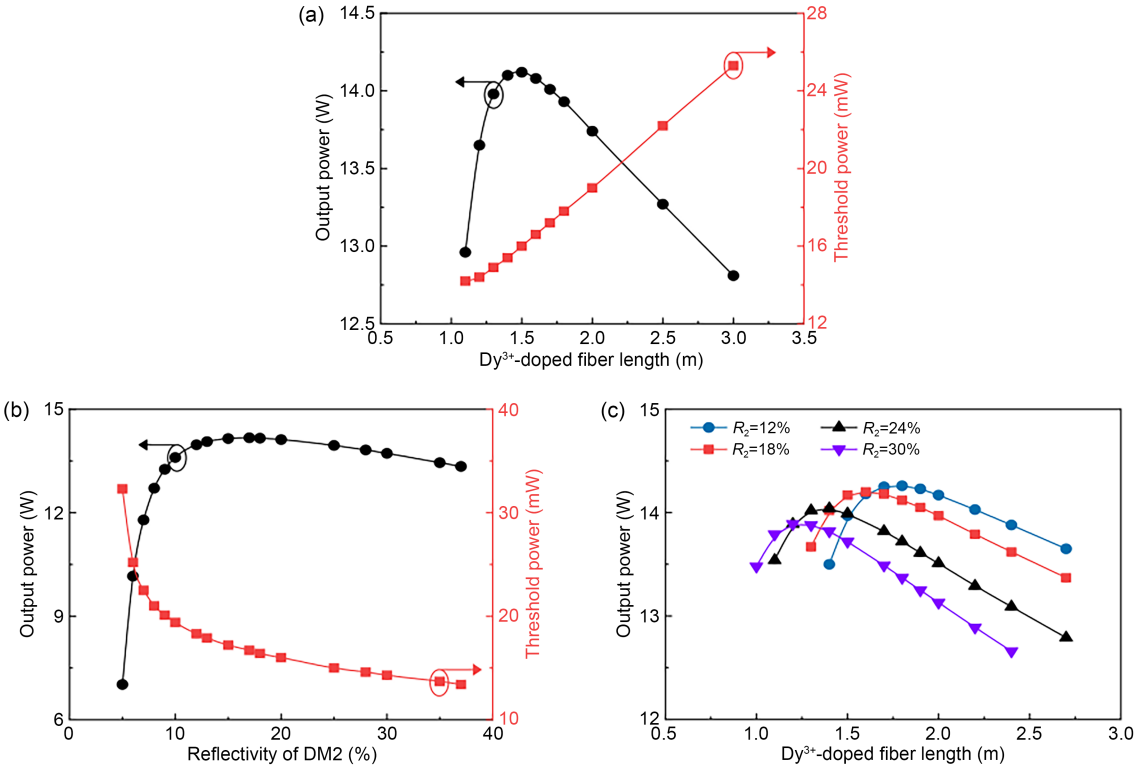

Fig. 3 Simulated output power and threshold power of the bi-directional pumped Dy^{3+}-doped fluoride fiber laser as a function of Dy^{3+}-doped fiber length (the overall incident pump power is 19 W and the output coupler reflectivity is 20%) (a), simulated output power and threshold power of the bi-directional pumped Dy^{3+}-doped fluoride fiber laser as a function of R_2 (the overall incident pump power is 19 W and the fiber length is 1.5 m) (b), and simulated output power of the bi-directional pumped Dy^{3+}-doped fluoride fiber laser versus the fiber length for R_2 values of 12%, 18%, 24%, and 30% (the overall incident pump power is 19 W) (c)

performance at an overall incident pump power of 19 W was investigated. Fig. 5 displays the output power as a function of the Dy^{3+}-doped fluoride fiber length for various dopant concentrations. As the dopant concentration of Dy^{3+} increases from 1.7×10^{25} to 7.26×10^{25} m^{-3}, the optimal fiber length for achieving the maximum output power decreases from 3.5 to 0.9 m, with the corresponding maximum output power increasing from 12.4 W to 15.3 W. These results indicate that higher efficiency can be achieved by selecting a gain fiber with a higher dopant concentration.

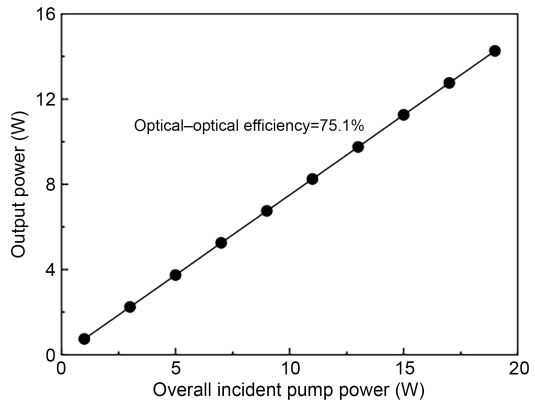

Fig. 4 Simulated output power of the bi-directional pumped Dy^{3+}-doped fluoride fiber laser as a function of the overall incident pump power under R_2=12% and L=1.8 m

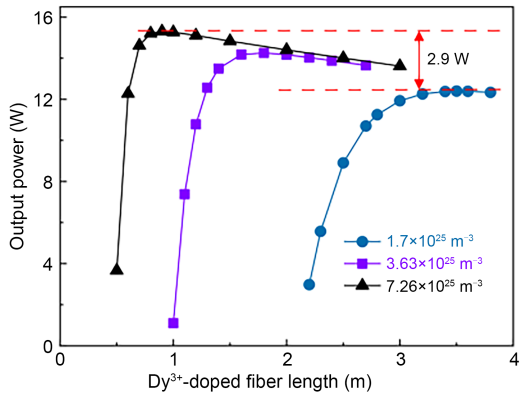

Fig. 5 Simulated output power of the bi-directional pumped Dy^{3+}-doped fluoride fiber laser as a function of the fiber length for different dopant concentrations (the overall incident pump power is 19 W and the output coupler reflectivity is 12%)

We would like to point out that the simulation results presented above were obtained based on the assumption of a fiber loss coefficient of 0.3 dBm^{-1}, which represents a large loss. Given the continuous advancements in fluoride fiber fabrication technology, it is anticipated that fibers with even lower loss coefficients can be produced. Under these improved conditions, one can expect higher efficiency in the Dy^{3+}-doped fluoride fiber laser. Furthermore, current research on the Dy^{3+}-doped fluoride fiber laser predominantly focuses on the continuous wave operation regime due to the lack of mid-IR saturable absorbers and dispersion compensation devices. The Dy^{3+}-doped fluoride fiber has demonstrated a broadband emission spanning from 2.8 to 3.4 μm, signifying its substantial potential for generating few-cycle mode-locked pulses (Wang YC et al., 2019). With the development of broadband saturable absorbers (Bharathan et al., 2019; Huang WC et al., 2020; Wang C et al., 2021; Hu et al., 2022; Qin et al., 2022; Pan et al., 2023; Wu et al., 2023) and dispersion compensation devices (Qin et al., 2019; Huang J et al., 2020), mode locking of the Dy^{3+}-doped fluoride fiber laser will garner increasing attention.

4 Conclusions

In summary, a bi-directional pumping scheme to address the limitation of output power scaling and to enhance the efficiency of the Dy^{3+}-doped fluoride fiber laser at 3.2 μm was investigated numerically based on rate equations and propagation equations. The simulations focused on exploring the impact of gain fiber length and reflectivity of the output coupler on the laser's performance. Detailed simulation results demonstrate that a maximum optical–optical efficiency of 75.1% with respect to the overall incident pump power can be achieved by optimizing the fiber and cavity parameters. Moreover, we identified the potential for further efficiency improvement by appropriately increasing the dopant concentration of Dy^{3+}. This work provides important guidance for achieving high-efficiency Dy^{3+}-doped fluoride fiber lasers in the high-power regime.

Contributors

Pinghua TANG and Yuchen WANG designed the research. Lingjing LI, Chunyang MA, and Nian ZHAO processed the data. Lingjing LI and Chunyang MA drafted the paper. Jie PENG, Bin LIU, and Haining JI helped organize the paper. Pinghua TANG and Yuchen WANG revised and finalized the paper.

Conflict of interest

All the authors declare that they have no conflict of interest.

Data availability

The data that support the findings of this study are available from the corresponding authors upon reasonable request.

References

Amin Z, Majewski MR, Woodward RI, et al., 2020. Novel near-infrared pump wavelengths for dysprosium fiber lasers. *J Lightw Technol*, 38(20):5801-5808. https://doi.org/10.1109/JLT.2020.3004428

Aydin YO, Fortin V, Vallée R, et al., 2018. Towards power scaling of 2.8 μm fiber lasers. *Opt Lett*, 43(18):4542-4545. https://doi.org/10.1364/ol.43.004542

Bharathan G, Jiang XT, Zhang H, et al., 2019. Mode-locked mid-IR fibre laser based on 2D nanomaterials. Proc SPIE 11200, AOS Australian Conf on Optical Fibre Technology (ACOFT) and Australian Conf on Optics, Lasers, and Spectroscopy (ACOLS), p.124-125. https://doi.org/10.1117/12.2539898

Crawford S, Hudson DD, Jackson SD, 2015. High-power broadly tunable 3-μm fiber laser for the measurement of optical fiber loss. *IEEE Photon J*, 7(3):1502309. https://doi.org/10.1109/JPHOT.2015.2430012

Falconi MC, Laneve D, Bozzetti M, et al., 2018. Design of an efficient pulsed Dy^{3+}: ZBLAN fiber laser operating in gain switching regime. *J Lightw Technol*, 36(23):5327-5333. https://doi.org/10.1109/JLT.2018.2871665

Faucher D, Bernier M, Androz G, et al., 2011. 20 W passively cooled single-mode all-fiber laser at 2.8 μm. *Opt Lett*, 36(7):1104-1106. https://doi.org/10.1364/OL.36.001104

Fortin V, Jobin F, Larose M, et al., 2019. 10-W-level monolithic dysprosium-doped fiber laser at 3.24 μm. *Opt Lett*, 44(3): 491-494. https://doi.org/10.1364/OL.44.000491

Hu Y, Wang MK, Hu LP, et al., 2022. Recent advances in two-dimensional graphdiyne for nanophotonic applications. *Chem Eng J*, 450:138228. https://doi.org/10.1016/j.cej.2022.138228

Huang J, Pang M, Jiang X, et al., 2020. Sub-two-cycle octave-spanning mid-infrared fiber laser. *Optica*, 7(6):574-579. https://doi.org/10.1364/OPTICA.389143

Huang WC, Ma CY, Li C, et al., 2020. Highly stable MXene (V_2CT_x)-based harmonic pulse generation. *Nanophotonics*, 9(8):2577-2585. https://doi.org/10.1515/nanoph-2020-0134

Ilev IK, Waynant RW, 2006. Mid-infrared biomedical applications. In: Krier A (Ed.), Mid-Infrared Semiconductor Optoelectronics. Springer, London, p.615-634. https://doi.org/10.1007/1-84628-209-8_19

Jackson SD, 2003. Continuous wave 2.9 μm dysprosium-doped fluoride fiber laser. *Appl Phys Lett*, 83(7):1316-1318. https://doi.org/10.1063/1.1603353

Jackson SD, 2012. Towards high-power mid-infrared emission from a fibre laser. *Nat Photon*, 6(7):423-431. https://doi.org/10.1038/nphoton.2012.149

Jobin F, Paradis P, Fortin V, et al., 2020. 1.4 W in-band pumped Dy^{3+}-doped gain-switched fiber laser at 3.24 μm. *Opt Lett*, 45(18):5028-5031. https://doi.org/10.1364/OL.398425

Jobin F, Paradis P, Aydin YO, et al., 2022. Recent developments in lanthanide-doped mid-infrared fluoride fiber lasers [Invited]. *Opt Express*, 30(6):8615-8640. https://doi.org/10.1364/OE.450929

Li JF, Jackson SD, 2012. Numerical modeling and optimization of diode pumped heavily-erbium-doped fluoride fiber lasers. *IEEE J Quantum Elect*, 48(4):454-464. https://doi.org/10.1109/JQE.2012.2183856

Li JF, Hudson DD, Liu Y, et al., 2012. Efficient 2.87 μm fiber laser passively switched using a semiconductor saturable absorber mirror. *Opt Lett*, 37(18):3747-3749. https://doi.org/10.1364/OL.37.003747

Luo HY, Wang YZ, Chen JS, et al., 2022. Red-diode-clad-pumped Er^{3+}/Dy^{3+} codoped ZrF_4 fiber: a promising mid-infrared laser platform. *Opt Lett*, 47(20):5313-5316. https://doi.org/10.1364/OL.470436

Luo HY, Shi JC, Chen JS, et al., 2023. Towards high-power and -efficiency ~2.8 μm lasing: lightly-erbium-doped ZrF fiber laser pumped at ~1.7 μm. *J Lightw Technol*, 42(1): 316-325. https://doi.org/10.1109/jlt.2023.3305608

Majewski MR, Jackson SD, 2016. Highly efficient mid-infrared dysprosium fiber laser. *Opt Lett*, 41(10):2173-2176. https://doi.org/10.1364/OL.41.002173

Majewski MR, Woodward RI, Jackson SD, 2018. Dysprosium-doped ZBLAN fiber laser tunable from 2.8 μm to 3.4 μm, pumped at 1.7 μm. *Opt Lett*, 43(5):971-974. https://doi.org/10.1364/OL.43.000971

Majewski MR, Amin Z, Berthelot T, et al., 2019. Directly diode-pumped mid-infrared dysprosium fiber laser. *Opt Lett*, 44(22):5549-5552. https://doi.org/10.1364/OL.44.005549

Majewski MR, Woodward RI, Jackson SD, 2020. Dysprosium mid-infrared lasers: current status and future prospects. *Laser Photon Rev*, 14(3):1900195. https://doi.org/10.1002/lpor.201900195

Majewski MR, Bharathan G, Fuerbach A, et al., 2021. Long wavelength operation of a dysprosium fiber laser for polymer processing. *Opt Lett*, 46(3):600-603. https://doi.org/10.1364/OL.417208

Pajewsk L, Sójka L, Lamrin S, et al., 2023. Experimental investigation of actively Q-switched Dy^{3+} doped fluoride single mode fiber laser operating near 3 μm. *J Lightw Technol*, 42(2):809-813. https://doi.org/10.1109/jlt.2023.3313620

Pan H, Chu HW, Li Y, et al., 2023. Bismuthene quantum dots integrated D-shaped fiber as saturable absorber for multi-type soliton fiber lasers. *J Materiom*, 9(1):183-190. https://doi.org/10.1016/j.jmat.2022.08.002

Qin ZP, Xie GQ, Gu HA, et al., 2019. Mode-locked 2.8-μm fluoride fiber laser: from soliton to breathing pulse. *Adv Photon*, 1(6):065001. https://doi.org/10.1117/1.AP.1.6.065001

Qin ZP, Chai XL, Xie GQ, et al., 2022. Semiconductor saturable absorber mirror in the 3–5 μm mid-infrared region. *Opt Lett*, 47(4):890-893. https://doi.org/10.1364/OL.444485

Quimby RS, Shaw LB, Sanghera JS, et al., 2008. Modeling of cascade lasing in Dy: chalcogenide glass fiber laser with efficient output at 4.5 μm. *IEEE Photon Technol Lett*, 20(2): 123-125. https://doi.org/10.1109/LPT.2007.912541

Shen YL, Wang YS, Chen HW, et al., 2017. Wavelength-tunable passively mode-locked mid-infrared Er^{3+}-doped ZBLAN fiber laser. *Sci Rep*, 7(1):14913. https://doi.org/10.1038/s41598-017-13089-6

Sijan A, 2009. Development of military lasers for optical countermeasures in the mid-IR. Technologies for Optical Countermeasures VI, p.32-45. https://doi.org/10.1117/12.835439

Sójka L, Pajewski L, Popenda M, et al., 2018. Experimental investigation of mid-infrared laser action from Dy^{3+} doped fluorozirconate fiber. *IEEE Photon Technol Lett*, 30(12): 1083-1086. https://doi.org/10.1109/LPT.2018.2832009

Sujecki S, 2014. An efficient algorithm for steady state analysis of fibre lasers operating under cascade pumping scheme. *Int J Electron Telec*, 60(2):143-149. https://doi.org/10.2478/eletel-2014-0017

Tang PH, Wang YC, Vicentini E, et al., 2022. Single-frequency Dy: ZBLAN fiber laser tunable in the wavelength range from 2.925 to 3.250 μm. *J Lightw Technol*, 40(8):2489-2493. https://doi.org/10.1109/JLT.2021.3138278

Tsang YH, El-Taher AE, 2011. Efficient lasing at near 3 μm by a Dy-doped ZBLAN fiber laser pumped at ~1.1 μm by an Yb fiber laser. *Laser Phys Lett*, 8(11):818-822. https://doi.org/10.1002/lapl.201110068

Tsang YH, El-Taher AE, King TA, et al., 2006. Efficient 2.96 micron dysprosium-doped ZBLAN fibre laser pumped at 1.3 micron. Solid State Lasers and Amplifiers II, p.156-165. https://doi.org/10.1117/12.666892

Wang C, Xu JW, Wang YZ, et al., 2021. MXene (Ti_2NT_x): synthesis, characteristics and application as a thermo-optical switcher for all-optical wavelength tuning laser. *Sci China Mater*, 64(1):259-265. https://doi.org/10.1007/s40843-020-1409-7

Wang YC, Jobin F, Duval S, et al., 2019. Ultrafast Dy^{3+}: fluoride fiber laser beyond 3 μm. *Opt Lett*, 44(2):395-398. https://doi.org/10.1364/OL.44.000395

Wang YZ, Luo HY, Gong HT, et al., 2022. Watt-level and tunable operations of 3 μm-class dysprosium ZrF_4 fiber laser pumped at 1.69 μm. *IEEE Photon Technol Lett*, 34(14): 737-740. https://doi.org/10.1109/LPT.2022.3183089

Wang ZH, Zhang B, Liu J, et al., 2020. Recent developments in mid-infrared fiber lasers: status and challenges. *Opt Laser Technol*, 132:106497. https://doi.org/10.1016/j.optlastec.2020.106497

Woodward RI, Gorjan M, 2022. Modeling mid-infrared fiber laser systems. In: Jackson S, Bernier M, Vallée R (Eds.), Mid-Infrared Fiber Photonics. Woodhead Publishing, London, England, p.743-801. https://doi.org/10.1016/B978-0-12-818017-4.00003-3

Woodward RI, Majewski MR, Bharathan G, et al., 2018. Watt-level dysprosium fiber laser at 3.15 μm with 73% slope efficiency. *Opt Lett*, 43(7):1471-1474. https://doi.org/10.1364/OL.43.001471

Wu Q, Wang YY, Zhao G, et al., 2023. 2 μm passively Q-switched Tm: YAG pulse laser with a graphdiyne saturable absorber. *Infrared Phys Technol*, 134:104914. https://doi.org/10.1016/j.infrared.2023.104914

Xiao Y, Xiao XS, He CJ, et al., 2024. Gain-switched 3 μm dysprosium-doped fluoride fiber laser pumped at 1.7 μm. *Opt Laser Technol*, 169:110162. https://doi.org/10.1016/j.optlastec.2023.110162

Ycas G, Giorgetta FR, Baumann E, et al., 2018. High-coherence mid-infrared dual-comb spectroscopy spanning 2.6 to 5.2 μm. *Nat Photon*, 12(4):202-208. https://doi.org/10.1038/s41566-018-0114-7

Zhang L, Zhang JX, Sheng Q, et al., 2022. High-efficiency thulium-doped fiber laser at 1.7 μm. *Opt Laser Technol*, 152: 108180. https://doi.org/10.1016/j.optlastec.2022.108180